H + Ar collisions. II. Differential scattering calculations*

H. Neumann, T. Q. Le, and B. Van Zyl
University of Denver, Denver, Colorado 80208
(Received 10 January 1977)

Differential elastic scattering cross-section calculations have been made for H + Ar collisions using classical and eikonal techniques. The calculation procedures are described and compared with existing experimental data. It is shown that the angular distribution of the elastic cross section is similar to that obtained for proton production in such collisions at energies above about 200 eV. By combining the angular dependence of the computed elastic cross section with experimental measurements described in the preceding paper, absolute differential cross sections for proton production have been determined.

I. INTRODUCTION

During the course of an experimental program to measure charged particle production cross sections for 50 eV to 3 keV hydrogen-atom collisions with argon atoms, it was found that fast, large-angle-scattered protons from the ionization-stripping reaction

$$H + Ar \rightarrow H^+ + e^- + Ar \qquad (1)$$

were contributing to the measured signals from other processes. A detailed discussion of the measurement problems which may be attributed to this effect is found in the preceding paper (paper I).[1]

In order to gain insight into this problem and to utilize fully the information contained in the various experimental signal measurements, a program of differential scattering calculations was carried out. These calculations not only enabled one to make more accurate determinations of the cross sections for Ar^+ formation, but, in combination with the experimental data, allowed a determination of the large-angle-scattering differential cross section for reaction (1).

Except for the lowest hydrogen-atom energies employed for the measurements ($\lesssim$100 eV), the scattering angles required for collisionally produced protons to contribute to the measurement difficulties ranged from about 10° to essentially 180°. For these large angles and over most of the energy range covered by the experiments, classical and semiclassical cross-section calculations are valid, at least to the accuracy required for interpretation of the measured data. Moreover, these large-angle-scattering collisions are rather hard interactions, occurring at small impact parameters. Accordingly, it was postulated that the angular distribution (though not necessarily the magnitude) of the proton production differential cross section ($d\sigma_{01}/d\Omega$) is similar to that of the elastic scattering cross section ($d\sigma_e/d\Omega$). (Evidence to support this postulate is presented in Sec. II.) As discussed in detail in paper I,[1] knowledge of the angular distributions alone is sufficient to enable the scattered proton contribution to be removed as an obstacle to the interpretation of the measured signals. In addition, this knowledge of the angular distribution can be combined with the experimental measurements to determine absolutely the $d\sigma_{01}/d\Omega$ cross section for reaction (1).

Many classical elastic scattering calculations have been described in the literature. For example, Smith, Marchi, and Dedrick[2] have derived forward and backward expansions of the reduced cross section $\theta \sin\theta\, \sigma(\theta, E)$ as a function of reduced scattering angle $E\theta$, for arbitrary potentials. Everhart, Stone, and Carbone[3] and Bingham[4] have provided extensive calculations for exponentially screened Coulomb potentials. Dose[5] performed calculations valid in the small-angle limit for H^+ and H on He, Ne, and Ar, utilizing as an interaction a convolution of a point proton or H(1s) charge distribution with an ion–target-atom potential due to Smith, Marchi, Aberth, Lorents, and Heinz[6] that employs different screening lengths for each electron shell. (This same interaction was adopted for the present calculations.) Rice and Bingham[7] calculated ion-atom cross sections for two interactions, the first a generalization to complex projectiles of the Smith *et al.*[6] screened-shell potential, and the second, a sum of the unperturbed interactions of the nuclear charge and Hartree-Fock-Slater electron densities of projectile and target. Common to all these calculations (and utilized in the present work) is the assumption that the charge distributions of projectile and target remain the same during the collision as they were at infinite separation. The validity of this approximation obviously decreases with decreasing energy.

In order to offset at least partially the angular-range limitations imposed by the classical description of the scattering process, eikonal cal-

culations were also carried out for smaller θ. These differential cross sections merged smoothly into their classical counterparts near the upper ends of the angular ranges in which they were made, even though they displayed moderate diffractional structure at smaller angles.

Because the experimental measurements required differential cross sections encompassing wide ranges in energy and angle for their interpretation, it was necessary to employ a relatively simple collision model and fast calculational procedures. The calculations are described in Sec. II, and their results are compared with previously measured differential elastic and inelastic [i.e., reaction (1)] cross sections. The techniques used to place $d\sigma_{01}/d\Omega$ on an absolute basis are presented in Sec. III. Certain details of the numerical procedures are found in the Appendix.

II. DIFFERENTIAL CROSS SECTION CALCULATIONS

Classical potential scattering calculations are valid provided[8] (a) the reduced wavelength $\lambda\!\!\!^{-}$ is small compared with the potential range a and (b) the diffractional deflection ($\approx \lambda\!\!\!^{-}/a$) is much smaller than the lesser of the scattering angle θ or unity.

For a repulsive interaction $U(r)$, the center-of-mass scattering angle θ is the same as the classical deflection function and is given by[9]

$$\theta = \pi - 2\int_{r_0}^{\infty} \frac{dr\rho}{r^2}\left[1-\frac{\rho^2}{r^2}-\frac{U(r)}{E}\right]^{-1/2}, \tag{2}$$

where ρ is the impact parameter and E the collision energy. The lower integration limit r_0 is the distance of closest approach, i.e., the (outermost) zero of the quantity in square brackets. Equation (2) implicitly provides ρ vs θ, from which the differential elastic scattering cross section is then given by

$$\frac{d\sigma_e}{d\Omega} = \frac{\rho}{\sin\theta}\left|\frac{d\rho}{d\theta}\right|. \tag{3}$$

The ρ-vs-θ information obtained by (numerical) integration of Eq. (2) was expressed in terms of an "effective" nuclear charge $Z_{\rm eff}(\theta)$, defined by the Coulomb-type expression

$$Z_{\rm eff}(\theta) = (2\rho E/e^2)\tan\tfrac{1}{2}\theta, \tag{4}$$

where e is the electronic charge. [For pure Coulombic interactions, $Z_{\rm eff}(\theta)$ reduces to the product of the atomic numbers of projectile and target.] To simplify calculations of the derivative in Eq. (3), the $Z_{\rm eff}(\theta)$ results were expressed in the form

$$Z_{\rm eff}(\theta) = \exp\left(\sum_{i=0}^{5} b_i[\ln(E\theta)]^i\right). \tag{5}$$

TABLE I. Expansion coefficients b_i for $Z_{\rm eff}(\theta)$ for H +Ar elastic collisions for Eq. (5). These values correspond to E measured in atomic units and θ in radians.

E (keV)	b_1	b_2	$10b_3$	10^2b_4	10^3b_5	10^4b_6
15	0.227	0.783	−0.492	−0.300	0.193	0.006
3	0.226	0.781	−0.497	−0.305	−0.168	0.403
2	0.225	0.780	−0.502	−0.353	−0.180	0.436
1	0.222	0.777	−0.518	−0.491	−0.097	0.374
0.5	0.217	0.771	−0.553	−0.643	−0.243	0.641
0.1	0.176	0.718	−0.827	−1.204	0.457	−5.521

The coefficients b_i were obtained by least-squares fits to the data of Eq. (4). The use of a six-term expansion was somewhat arbitrary, but designed to assure sufficient accuracy of the fit. Generally, the rms residuals for the $Z_{\rm eff}(\theta)$ fit were well under 0.01, while typical $Z_{\rm eff}(\theta)$ values ranged upward from 2. Table I displays the values of the coefficients b_i at selected energies. The first four coefficients, which vary systematically with energy, are significant in the expansion. The last two, which are quite small, fluctuate somewhat and add only a little to the quality of the fit at most energies.

Further details of the numerical procedures used to evaluate the scattering angle are given in the Appendix.

In order to obtain elastic cross sections for small θ, in the diffractional range, eikonal calculations[8(b)] were carried out. The small-angle scattering amplitude

$$f(\theta) = -ik\int_0^{\infty} d\rho\,\rho J_0(k\rho\theta)\{\exp[2i\chi(\rho)]-1\}, \tag{6}$$

where $k = 1/\lambda\!\!\!^{-}$, with eikonal phase shift

$$\chi(\rho) = -\frac{k}{2E}\int_0^{\infty} dr\, r(r^2-\rho^2)^{-1/2}\,U(r) \tag{7a}$$

$$= -\frac{ke^2}{2E}\sum_n \alpha_n[(1-c_n^2)K_0(\rho/a_n) + c_n^2K_0(2\rho/a_0) + c_n(\rho/a_0)K_1(2\rho/a_0)], \tag{7b}$$

was evaluated by numerical integration for the range $0 \le \theta \le 10°$. The differential cross sections, the absolute squares of $f(\theta)$, fit smoothly in all cases onto the classical cross sections for $\theta \lesssim 10°$ and displayed some diffractional structure at smaller angles. The expression given in Eq. (7b) is Eq. (7a) evaluated for the interaction given in Eq. (11), below; $K_m(z)$ is the modified Bessel function of the second kind of order m and argument z.[10]

Following the procedure proposed by Dose,[5] the interaction is here taken to be

$$U(r) = \int d\tau\, \rho_H(\vec{r}_2) V(r_1), \tag{8}$$

where the integration is performed over all space, the hydrogen-atom charge distribution being given by a point proton nucleus and the square of the H(1s) electronic wave function; thus

$$\rho_H(\vec{r}_2) = e[\delta(\vec{r}_2) - (1/\pi a_0^3)\exp(-2r_2/a_0)], \tag{9}$$

where a_0 is the first Bohr radius. The Ar target-atom potential is taken to be

$$V(r_1) = \frac{e}{r_1}\sum_n \alpha_n \exp(-r_1/a_n). \tag{10}$$

In Eq. (10), the sum ranges over K, L, and M shells ($\alpha_n = 2, 8, 8$, respectively), and the screening lengths a_n (0.057, 0.18, and 0.93 bohr) are determined from $a_n = (I_H/I_n)^{1/2} a_0$, where I_H is the atomic hydrogen ionization energy and I_n is the ionization energy for the nth shell. This potential was found by Smith *et al.*[6] to allow a good fit to $He^+ + Ne$ and $He^+ + Ar$ scattering data over a substantial energy and angular range.[11] This interaction may be integrated analytically; the result is[5]

$$U(r) = e^2 \sum_n \alpha_n[(1 - c_n^2)\exp(-r/a_n)/r + c_n(1/a_0 + c_n/r)\exp(-2r/a_0)], \tag{11}$$

where $c_n = 1/[1 - (a_0/2a_n)^2]$.

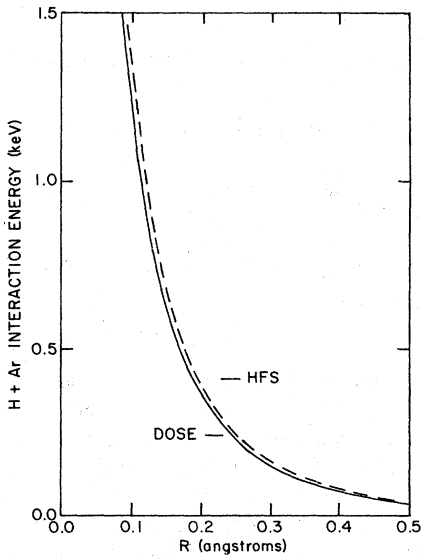

FIG. 1. H+Ar interaction energy. The solid curve is Dose's (Ref. 5) interaction and is calculated from Eq. (11). The dashed curve is the interaction of a ground-state hydrogen atom with the sum of the electrostatic potentials of the nucleus and a Hartree-Fock-Slater electron distribution for argon.

As a check, this interaction was compared numerically with one calculated for hydrogen atoms in the electrostatic potential of the nucleus and Hartree-Fock-Slater electron distribution for argon computed by Clementi and Roetti.[12] For $U(r) \gtrsim 25$ eV ($r \lesssim 1$ bohr), the range of primary interest in the present work, the two interactions agree to within about 7%, as shown in Fig. 1. In view of this agreement, and because the Hartree-Fock-Slater calculation requires far more computer time (even though it may be written down analytically as a collection of three-, four-, and five-fold sums), the simpler form, Eq. (11), was used for the numerous cross-section calculations of this study. Despite the good agreement between experimental and calculated cross sections found by Smith *et al.*[6] for $He^+ + Ne$ and $He^+ + Ar$ scattering and in the present study for H+Ar scattering, it should be borne in mind that the $U(r)$ of Eq. (11) incorporates neither inelastic nor charge polarization contributions, which should rapidly become more important at scattering energies below a few hundred eV.

There are two previous experiments involving argon targets against which the calculational procedure of this paper may be tested. Thomas, Leatherwood, and Harriss[13] have measured the differential elastic scattering cross section for 15-keV hydrogen atoms on argon. Their results, to which they assign an accuracy of ±14%, together with the present calculations, are shown in Fig. 2. It should be noted that the calculations here involve

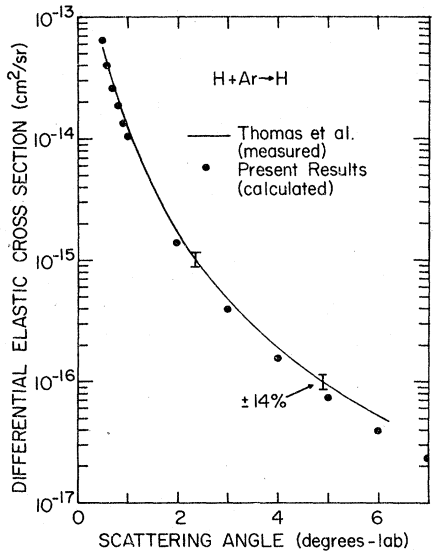

FIG. 2. H+Ar differential elastic cross sections at 15 keV. Solid circles are present calculation. Curve shows the experimental results, including error flags, of Thomas *et al.* (Ref. 13).

no adjusted parameters and are not normalized to the experimental values. The agreement in both magnitude and angular distribution is quite satisfactory.

Figure 3 shows the results of the present calculations (with the absolute value of $d\sigma_{01}/d\Omega$ having been determined by the procedure to be described in the next section) as determined for proton production in 1-keV H+Ar collisions. Shown for comparison are the experimental results of Fleischmann, Barnett, and Ray,[14] who measured the relative angular dependence for this differential inelastic cross section. Their data have been normalized to the present results at a scattering angle of about 4°.

Note the rather striking agreement between the angular dependencies of the calculated and experimental cross sections. Since the calculated results implicitly contain the angular dependence of the elastic scattering computations, the authors conclude that the angular dependencies of $d\sigma_e/d\Omega$ and $d\sigma_{01}/d\Omega$ are indeed quite similar. While this situation is certain to deteriorate at very low energies, the close agreement at 1 keV lends support to the extension of the present $d\sigma_{01}/d\Omega$ determination procedure down into the few hundred eV range.

III. ABSOLUTE NORMALIZATION OF THE PROTON PRODUCTION DIFFERENTIAL CROSS SECTION

With the procedure for determining the angular dependence of the proton production cross section

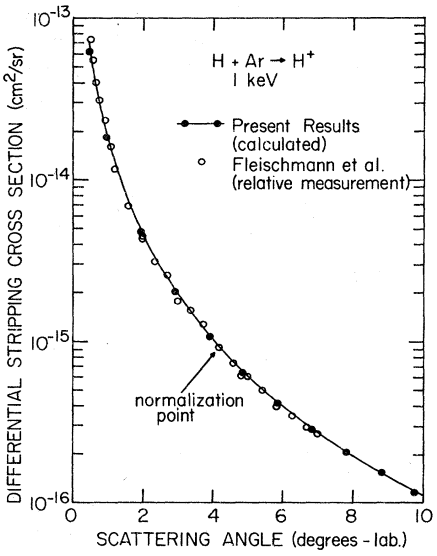

FIG. 3. H+Ar differential stripping cross section at 1 keV. Solid circles, present results; open circles, relative angular distribution measured by Fleischmann *et al.* (Ref. 14), normalized to present results at approximately 4°.

($d\sigma_{01}/d\Omega$) established, the technique by which the cross section can be placed on an absolute basis can now be discussed. As this technique involves intercomparison between the calculations described above and the measurements described in paper I,[1] the reader is referred to Sec. III of that paper for the details of the procedure.

In summary, the technique involves utilizing the differential scattering calculations and the measured signals to collector B (see Fig. 1 of paper I) to obtain an absolute value for the "composite proton scattering cross section" to collector B. This essentially experimental quantity must be given by

$$\sigma_{pB}^{+}=\frac{1}{L}\int_0^X\left(\int_{\Delta\Omega_B(x,\theta,\phi,V)}F(x,\theta)\frac{d\sigma_{01}}{d\Omega}d\Omega\right)dx\,, \quad (12)$$

the second term of Eq. (11) in paper I, where the various symbols used are defined. In essence, σ_{pB}^{+} represents a measure of the protons, having been produced a depth x into the target cell, and scattered at angles θ and ϕ, that will arrive at collector B under the influence of the target-cell electric fields symbolized by V.

A calculated "composite hydrogen-atom scattering cross section" σ_{hB}^{+} can be obtained by substituting the computed $d\sigma_e/d\Omega$ into Eq. (12) for $d\sigma_{01}/d\Omega$ and executing the integrals indicated.[15] The absolute value of $d\sigma_{01}/d\Omega$ may then be found from the ratio

$$\frac{d\sigma_{01}/d\Omega}{d\sigma_e/d\Omega}\equiv\frac{\sigma_{pB}^{+}}{\sigma_{hB}^{+}}. \quad (13)$$

Plots of σ_{pB}^{+} and σ_{hB}^{+} are shown in Fig. 4 as functions of the hydrogen-atom collision energy.

The upper curve in Fig. 4 shows the calculated

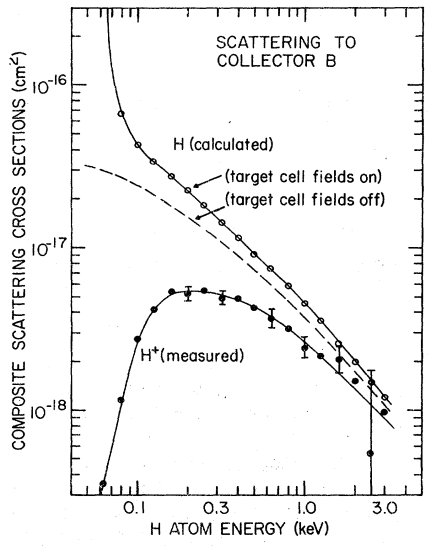

FIG. 4. Composite scattering cross sections to positive charge collector B. See discussion in text.

σ^+_{hB}. Note that this "composite scattering cross section" falls off with increasing energy with an energy dependence slightly stronger than E^{-1} at energies in excess of about 100 eV. Below this value, σ^+_{hB} increases rapidly, a measure of the fact that the target-cell collection fields are sufficiently high relative to the beam energy to allow collection of essentially forward scattered particles.[15]

To determine the effects of the target-cell collection fields on the scattering-plus-collection process, the computation of σ^+_{hB} was repeated with fields (mathematically) set to zero. The dashed curve in Fig. 4 gives the results of this calculation. The difference between this curve and the upper curve shows that it is important to incorporate the collection field effects into the analysis, especially at the lower energies.

The lower curve shows the results obtained for σ^+_{pB}. As discussed in paper I[1] in Sec. III, it is actually possible to obtain six independent measures of this "composite scattering cross section" at energies above 400 eV, and three independent measures between 200 and 400 eV. The flags shown on the σ^+_{pB} represent the standard deviations of these independent measurements. As these independent determinations emphasize substantially different angular ranges for scattering within the target cell, the agreement between the various determinations at each energy provides further evidence that the angular dependencies of $d\sigma_e/d\Omega$ and $d\sigma_{01}/d\Omega$ are basically similar.

The typically large flag shown at 2.5 keV, however, results from the fact that at higher energies, the scattered proton signal to collector B is substantially smaller than the slow positive-ion signal (Ar^+). Thus the statistical uncertainties here arise largely from subtraction of two large numbers to obtain a comparatively small difference,[16] and do not reflect an inadequacy in the calculated angular scattering distribution.

As noted in Eq. (13), the absolute normalization of $d\sigma_{01}/d\Omega$ depends upon the ratio of the lower curve to the upper curve of Fig. 4. This ratio, which is about 0.7 at the higher energies, suggests that the two large-angle differential cross sections are comparable in magnitude in this energy range; i.e., the scattering event is insensitive to the charge state of the outgoing particle for these hard interactions. At the lower energies, this ratio begins to decrease monotonically, reaching a value of about 0.2 just below 200 eV, and falling rapidly thereafter. (This result is, of course, expected as the proton production inelasticity becomes more important to the collision kinematics.) It is surprising, however, that even at 200 eV, the large-angle differential scattering cross sections are close enough in magnitude to suggest a considerable similarity between these two reaction types.

APPENDIX

The integrals for Eq. (2) were carried out by first transforming the variable of integration to $u = 1/r$. The upper limit $u_{max} = 1/r_0$ was found by a Newton-Raphson search for the root of

$$F(u) = 1 - \rho^2 u^2 - U/E . \tag{A1}$$

To achieve better accuracy near u_{max}, the integration range was divided into two parts, $(0, u_{max}/2)$ and $(u_{max}/2, u_{max})$, and the contribution of the singularity at u_{max} subtracted before numerical integration and added back analytically. Thus Eq. (2) becomes

$$\theta = \pi - 2\rho\left\{\int_0^{u_{max}/2} du\, F^{-1/2}(u) + \int_{u_{max}/2}^{u_{max}} du\left[F^{-1/2}(u) - \left(\frac{dF}{du}\bigg|_{u_{max}}(u-u_{max})\right)^{-1/2}\right] + \left(-2u_{max}\Big/\frac{dF}{du}\bigg|_{u_{max}}\right)^{1/2}\right\}. \tag{A2}$$

The two integrals remaining were calculated by a high-order Gauss-Legendre procedure. The required derivative, which is negative, was available as a by-product of the root search.

*Supported in part by the Atmospheric Sciences Section of the National Science Foundation under Grant No. DES73-00654.

[1]B. Van Zyl, T. Q. Le, H. Neumann, and R. C. Amme, preceding paper, Phys. Rev. A 15, 1871 (1977). This paper is hereafter referred to as paper I.

[2]F. T. Smith, R. P. Marchi, and K. G. Dedrick, Phys. Rev. 150, 70 (1966).

[3]E. Everhart, G. Stone, and R. J. Carbone, Phys. Rev. 99, 1287 (1955).

[4]F. W. Bingham, J. Chem. Phys. 46, 2003 (1967); Natl. Bur. Std. (U.S.) Document No. SC-RR-66-506, 1966 (unpublished).

[5]V. Dose, Helv. Phys. Acta 41, 261 (1968). The present authors confirm the observation by Rice and Bingham (Ref. 7) that the numerical factors 32 and 8 in $U(r)$ in this paper should be 16 and 4, respectively; correspondingly, the factors 16 and 8 in τ should be 8 and

4, respectively.

[6]F. T. Smith, R. P. Marchi, W. Aberth, D. C. Lorents, and O. Heinz, Phys. Rev. 161, 31 (1967); F. T. Smith, in *Proceedings of the Fifth International Conference on the Physics of Electronic and Atomic Collisions: Abstracts of Papers*, edited by I. P. Flaks (Nauka, Leningrad, 1967), p. 181.

[7]J. K. Rice and F. W. Bingham, Phys. Rev. A 5, 2134 (1972).

[8](a) N. F. Mott and H. S. W. Massey, *The Theory of Atomic Collisions* (Oxford U.P., London, 1965), 3rd ed., Chap. V, Sec. 6; (b) R. C. Newton, *Scattering Theory of Waves and Particles* (McGraw-Hill, New York, 1966), Chap. 18.

[9]Reference 8(a), Chap. V, Sec. 5.

[10]G. N. Watson, *Theory of Bessel Functions* (Cambridge U.P., Cambridge, 1966), 2nd ed., Sec. 3.7.

[11]The calculations of Smith *et al.* were actually carried out for He^{++} projectiles on Ne and Ar. The fact that satisfactory fits were achieved to data for He^{++} projectiles suggests that for relatively hard collisions on complex targets, the initial charge state for low-Z projectiles is of only secondary importance. This implication is consistent with the postulate of the present paper, that the elastic scattering and stripping angular distributions should be quite similar, for hard collisions.

[12]E. Clementi and C. Roetti, At. Data Nucl. Data Tables 14, 178 (1974).

[13]E. W. Thomas, L. A. Leatherwood, and J. E. Harriss, Phys. Rev. A 12, 1835 (1975).

[14]H. H. Fleischmann, C. F. Barnett, and J. A. Ray, Phys. Rev. A 10, 569 (1974).

[15]For these calculations, the product scattered H atom was allowed to respond to the target-cell potentials as a product proton does.

[16]This situation can be seen by the results shown in Fig. 7 of paper I. Here the "composite proton scattering cross sections" to all positive charge collectors are merely the differences between the measured cross sections to the various collectors, and σ_{Ar^+}.